Steady-State Error Reduction with Fuzzy Gain Scheduling Integrator

Ali Kazemy[†], Seyed Amin Hosseini[†] and Mohammad Farrokhi[†,‡]
[†] Faculty of Electrical Engineering
[‡] Center of Excellence for Power System Automation and Operation
Iran University of Science and Technology, Tehran, Iran
ali_kazemy@ee.iust.ac.ir, amin_hosseini@ee.iust.ac.ir, farrokhi@iust.ac.ir

***Abstract* — In this paper, first, the dynamic equations of a submarine periscope will be extracted and verified with real data. These data are acquired from an experimental setup. Then, using a neural network, an intelligent control method will be developed to control the periscope model. For steady state error reduction of the main controller a Fuzzy Gain Scheduling (FGS) integrator scheme has been used. This integrating controller is parallel to the main controller. The main issue is to adjust the integrator gain using fuzzy logic to decrease the steady-state error, while maintaining stability of the closed-loop system. Fuzzy IF-THEN rules are used to adjust the gain of the integrator based on the tracking error and its derivative. Simulation results on the plant model indicate good performance of the proposed method.**

***Index Terms* — Marine systems, Fyzzy systems, Neural control, Scheduling algorithms, Kinematics.**

I. INTRODUCTION

Line-of-Site (LOS) stabilization has been widely used by many researchers for varieties of applications. Periscope, which is important equipment in submarines, is an optical instrument, which is considered to be an LOS device. In periscopes, image sequences, taken by a camera, must be stabilized for better views by operators [1]. A common periscope structure has been depicted in Figure 1. Image sequences, taken from the sea surface, are reflected by the mirror to the camera, and observed inside the submarine by the operator. Structure of a periscope is like the gyro mirror LOS stabilization [2]. Major application of periscope is in submarines but tanks use them too.

Extracting dynamic equations of submarine periscopes has advantageous for research, computer simulation and model-based controller design. The structure of this system is like a robot manipulator. Therefore, to obtain the dynamic equations, one can use the well-known methods like the Newton-Euler and Lagrange-Euler methods. In this paper, the latter method is employed.

Gain scheduling is an important form of nonlinear control methods in many applications areas, such as in commercial and military flight control, jet engine control, missile control, vehicular engine control and process control [3]. One technique to define gain scheduling is fuzzy logic, which is based on human knowledge [4]. The main advantage of this method is that the control law can be presented as IF-THEN rules using human expertise.

One of the simple techniques in classical control methods, to reduce steady-state error, is using integral term in control law. But the main difficulty is defining precise integrator gain, especially for highly nonlinear systems. It is well known that high integrator gains can push steady-state error towards zero; but any sudden changes in the reference signal and/or system parameters can jeopardize stability of the system.

In this paper, fuzzy logic is employed to define integrator gain in on-line method, in order to considerably reduce the steady-state error. Hence, the fuzzy gain integrator is in parallel with the controller for better performance at the steady state. In this paper, the main controller is a neural network.

The proposed method is applied to the extracted periscope model.

Although the proposed compensator will be applied to an image stabilization problem, it can be applied to other control methods for steady-state error reduction.

This paper in organized as follows. Section II describes forward kinematics of a typical periscope followed by derivation of dynamic equations in section III. Section IV describes the main controller, which is a neural network. Section V gives the proposed method (i.e. the fuzzy gain-scheduling integrator). Simulation results are shown in section VI, followed by conclusions in section VI**I.**

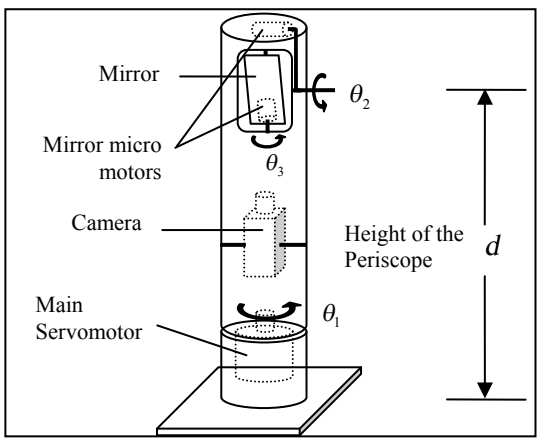

Fig. 1. Structure of a submarine periscope

II. Forward Kinematics

For obtaining the homogeneous transformation matrices, the basic method is used. Figure 2 shows the link coordinate frames of the periscope shown in Fig. 1. The transformation matrices of three links are defined as follows:

$$ {}^{0}T_{1}=\begin{bmatrix} c_1 & -s_1 & 0 & 0 \\ s_1 & c_1 & 0 & 0 \\ 0 & 0 & 1 & 0 \\ 0 & 0 & 0 & 1 \end{bmatrix} \quad {}^{1}T_{2}=\begin{bmatrix} c_2 & -s_2 & 0 & 0 \\ 0 & 0 & 1 & 0 \\ -s_2 & -c_2 & 0 & d \\ 0 & 0 & 0 & 1 \end{bmatrix} $$
$$ {}^{2}T_{3}=\begin{bmatrix} c_3 & -s_3 & 0 & 0 \\ 0 & 0 & -1 & 0 \\ s_3 & c_3 & 0 & 0 \\ 0 & 0 & 0 & 1 \end{bmatrix} \quad (1) $$

where ${}^{0}T_{1}$ is the transformation matrix from coordinate one to coordinate zero (the base coordinate), $c_1=\cos(\theta_1)$, $s_1=\sin(\theta_1)$ and so on.

III. Dynamic Equations of Periscope

To derive the dynamic equations, the Lagrange-Euler method is employed [5]. Hence, the kinetic and the potential energy of the all links must be determined.

A. The Potential and Kinetic Energy of the First Link

Since the body of periscope is fixed, the kinetic energy of the first link is just due to the energy of the servo motor. Equations (2) and (3) represent the kinetic and the potential energy of the first link, respectively.

$$ k_1=\frac{1}{2}J_1\dot{\theta}_1^2=\frac{1}{2}J_1\omega_1^2 \quad (2) $$

$$ p_1=\frac{1}{2}m_1gd \quad (3) $$

where J_1 and ω_1 are the moment of inertia and the angular velocity of the first link, respectively, and d is the height of periscope (Fig. 1).

B. The Potential and Kinetic Energy of the Second Link

The movement of the second link is like a see-saw. Hence, for finding the kinetic and potential energy of this link, it is divided in two pieces, with half mass on either side. After finding the kinetic and potential energy of each piece, the kinetic energies will be added together and the potential energies will be subtracted from each other, to find the kinetic and potential energy of the whole link. The velocity of the second link is calculated at $y_2=-b/2$ with respect to the first coordinate system, where b is depicted in Fig. 2. Equation (4) represents the position of this coordinate with respect to the zero coordinate system.

$$ \begin{bmatrix} x_2 \\ y_2 \\ z_2 \end{bmatrix}={}^{0}T_{1}{}^{1}T_{2}\begin{bmatrix} 0 \\ -\frac{b}{2} \\ 0 \\ 1 \end{bmatrix}=\begin{bmatrix} \frac{1}{2}bc_1s_2 \\ \frac{1}{2}bs_1s_2 \\ \frac{1}{2}bc_2+d \end{bmatrix} \quad (4) $$

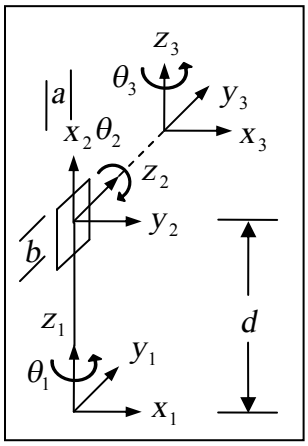

Fig. 2. Link coordinate frames of the periscope, shown in Fig. 1.

The velocity of the upper piece is equal to the velocity of the lower piece.

$$ v_2^2=\dot{x}_2^2+\dot{y}_2^2+\dot{z}_2^2=\frac{1}{4}b^2\left(\omega_1^2s_2^2+\omega_2^2\right). \quad (5) $$

Therefore, the kinetic energy of the second link is equal to

$$ k_2=2\left(\frac{1}{2}m_2v_2^2\right)+\frac{1}{2}J_2\omega_2^2=\frac{1}{4}m_2b^2\left(\omega_1^2s_2^2+\omega_2^2\right)+\frac{1}{2}J_2\omega_2^2. \quad (6) $$

The potential energy of the second link is equal to

$$ p_2=\frac{1}{2}m_2gz_{21}-\frac{1}{2}m_2gz_{22}=\frac{1}{2}m_2gbc_2. \quad (7) $$

C. The Potential and Kinetic Energy of the Third Link

The third link is treated like the second link. Equation (8) represents the position of the right half piece of the mirror coordinate.

$$ \begin{bmatrix} x_3 \\ y_3 \\ z_3 \end{bmatrix}={}^{0}T_{1}{}^{1}T_{2}{}^{2}T_{3}\begin{bmatrix} 0 \\ \frac{a}{2} \\ 0 \\ 1 \end{bmatrix}=\begin{bmatrix} \frac{1}{2}a\left(-c_1c_2s_3-s_1c_3\right) \\ \frac{1}{2}a\left(-s_1c_2s_3+c_1c_3\right) \\ \frac{1}{2}as_2s_3+d \end{bmatrix} \quad (8) $$

Hence, the velocity of this link is equal to

$$ \begin{aligned} v_3^2=\dot{x}_3^2+\dot{y}_3^2+\dot{z}_3^2=\frac{1}{4}a^2(&\omega_3^2+\omega_2^2+\omega_1^2c_2^2-\omega_1^2c_2^2c_3^2 \\ &+2\omega_1\omega_3c_2+\omega_1^2c_3^2-2\omega_1\omega_2s_2s_3c_3-\omega_2^2c_3^2). \end{aligned} \quad (9) $$

And the kinetic and potential energy of this link is

$$ k_3=2\left(\frac{1}{2}m_3v_3^2\right)+\frac{1}{2}J_3\omega_3^2, \quad (10) $$

$$ p_3=\frac{1}{2}m_3gz_{31}-\frac{1}{2}m_3gz_{32}=\frac{1}{2}m_3gas_2s_3. \quad (11) $$

D. Lagrangian Equation

The Lagrangian equations for the periscope can be written as

$$ \begin{cases} L=k_1+k_2+k_3-p_1-p_2-p_3 \\ \frac{\partial}{\partial t}\left(\frac{\partial L}{\partial \dot{\theta}}\right)-\frac{\partial L}{\partial \theta}=\tau. \end{cases} \quad (12) $$

Solving (13) yields dynamic equations as

$$\tau_1 = \left(J_1 + \frac{1}{2}m_2b^2s_2^2 + \frac{1}{2}m_3a^2\left(c_2^2 - c_2^2c_3^2 + c_2 + c_3^2\right)\right)\ddot{\theta}_1 +$$
$$+\left(\frac{1}{2}m_3a^2c_2\right)\ddot{\theta}_3 + \left(-\frac{1}{2}m_3a^2s_2s_3c_3\right)\ddot{\theta}_2 + m_2b^2\omega_1\omega_2s_2c_2$$
$$+\frac{1}{2}m_3a^2(-2\omega_1\omega_2s_2c_2 + 2\omega_1\omega_2c_2s_2c_3^2 + 2\omega_1\omega_3c_3s_3c_2^2$$
$$-2\omega_2\omega_3s_2 - 2\omega_1\omega_3c_3s_3 - \omega_2^2c_2c_3s_3 - \omega_2\omega_3s_2c_3^2$$
$$+\omega_2\omega_3s_2s_3^2),$$
$$\tau_2 = \left(-\frac{1}{2}m_3a^2s_2s_3c_3\right)\ddot{\theta}_1 + \left(J_2 + \frac{1}{2}m_2b^2 + \frac{1}{2}m_3a^2\right)\ddot{\theta}_2$$
$$+\frac{1}{2}m_3a^2(2\omega_1\omega_2c_2c_3s_3 - \omega_1\omega_3s_2c_3^2 + \omega_1\omega_3s_2s_3^2$$
$$+2\omega_3c_3s_3 + \omega_1^2c_2s_2 - \omega_1^2c_2s_2c_3^2 + \omega_1\omega_3s_2 \qquad (13)$$
$$+\omega_1\omega_2c_2c_3s_3) - \frac{1}{2}m_2b^2\omega_1^2s_2c_2 - \frac{1}{2}m_2gbs_2$$
$$+\frac{1}{2}m_3gac_2s_3,$$
$$\tau_3 = \left(\frac{1}{2}m_3a^2c_2\right)\ddot{\theta}_1 + \left(J_3 + \frac{1}{2}m_3a^2\right)\ddot{\theta}_3 + \frac{1}{2}m_3gas_2c_3$$
$$+\frac{1}{2}m_3a^2(-\omega_1\omega_2s_2 - \omega_1^2c_3s_3c_2^2 + \omega_1^2c_3s_3$$
$$+\omega_1\omega_2s_2c_3^2 - \omega_1\omega_2s_2s_3^2 - \omega_2c_3s_3).$$

Dynamic of the servomotors are as follows

$$\dot{I}_a = \frac{1}{L_a}\left(-R_aI_a - k_b\dot{\theta}_M + v_a\right)$$
$$\tau_M = -J\ddot{\theta}_M - B_M\dot{\theta}_M + k_aI_a \qquad (14)$$

Motor and plant parameters are written in table I and II, respectively. A comparison between the data acquired from an experimental system (Fig. 3) and the proposed model in this paper, taking the dynamics of servomotors into account, has been depicted in Fig. 4. The modeling error has been shown in Fig. 5. As this figure shows, the error between the experimental data and proposed model is relatively very small.

Fig. 3. Experimental setup

TABLE I
MOTOR PARAMETERS

$R_a\ (\Omega)$	L_a (mH)	K_b (mV/rpm)	K_a (mNm/A)
40.2	0.8	3.2	35.1

TABLE II
PLANT PARAMETERS

$m_1(kg)$	m_2	m_3	$a(m)$	$b(m)$	$d(m)$
30	0.08	0.5	0.03	0.08	1.1

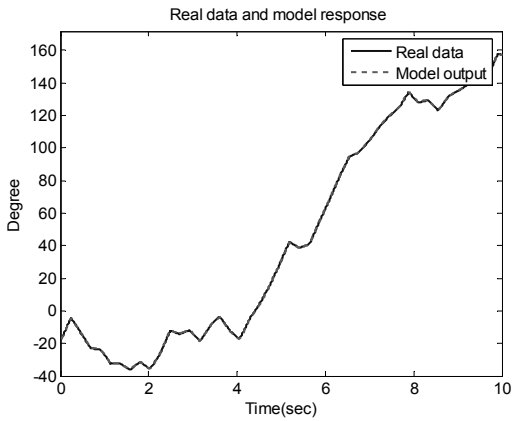

Fig. 4. Comparison of real and model response

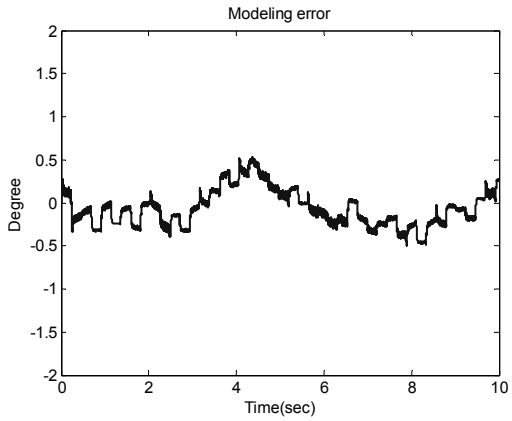

Fig. 5. Modeling error

IV. THE MAIN CONTROLLER

An MLP neural network is the main controller to control the nonlinear system. This network consists of an input layer, one or two hidden layers, and an output layer (Fig. 1). The mathematical equations of the MLP, with one output and one hidden layer, can be written as

$$y = \rho\left(\sum_j w_j^O Q_j + b^O\right),\ Q_j = \rho\left(q_j\right) \qquad (15)$$

$$q_j = \sum_i w_{ij}^I u_i + b_j^I\ ,\ \rho(\cdot) = \frac{1}{1+e^{-(\cdot)}}. \qquad (16)$$

where y and u are the output and input of the NN, W_{ij}^I and W_j^O are the hidden and output layer weigths and finally b_j^I and b^O are the hidden and output layer bias weights.

Error backpropagation training algorithm is the most common method used in literature to train MLP neural networks; hence, the same training method has been employed in this paper to control the nonlinear plant.

The NN will be trained off-line, using some data acquired from the plant, to obtain an inverse model of the system. Then, the trained NN is used as the main controller in the closed-loop system. In order to obtain a very accurate inverse model of a highly nonlinear system, one would need many neurons in the hidden

layer of NN. On the other hand, too many neurons might hinder real-time control in most applications.

For controlling the plant, we should train the neural network with plant data in off-line case. Unfortunately, the numbers of neurons are few and the neural network can not capture the complete dynamic response of the plant, which causes some steady state error in reference tracking.

To compensate the steady-state error, an integral term will be added to the control signal. It is well known that integral term can push the steady-state to very small numbers. But the gain of the integral term is very crucial. Small gains are not very effective, and large gains may destabilize the system, when some changes occur in the system parameters. In the next section, a gain scheduling will be presented, which adjusts the integral gain according to the performance of the closed-loop response.

V. Fuzzy Gain Scheduling Structure

Figure 6 shows the control block diagram. Inputs of the fuzzy system are the tracking error and its derivative. Experience shows that with decreasing the tracking error and its derivative we should increase the integrator gain for reducing the steady state error. Therefore it is obvious that the membership functions for the inputs should be concentrated around zero. Moreover, the fuzzy IF-THEN rules must be selected in such a way that the fuzzy output surface be a mountain like with large slops. Figs. 7, 8 and 9 show the membership functions for the inputs and the output, respectively. Fuzzy rules are given in Table III. Also fuzzy output surface is depicted in Fig. 6. In the structure of the fuzzy system, the Mamdani product inference engine, singleton fuzzifier, and center average defuzzifier is used.

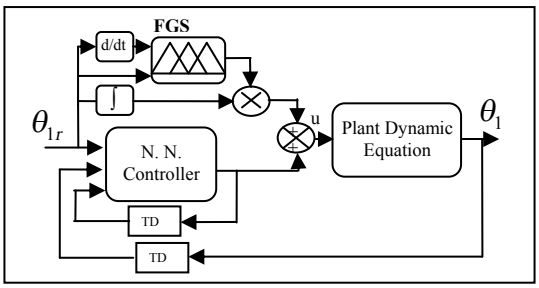

Fig. 6. Control block diagram

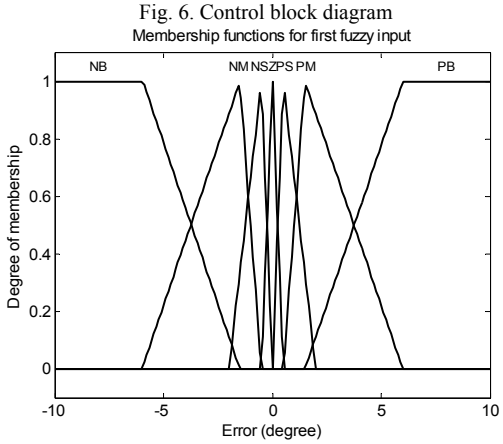

Fig. 7. Membership functions for the error input

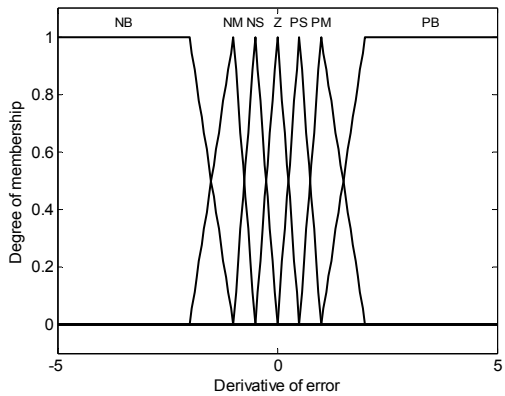

Fig. 8. Membership functions for the derivative of the error input

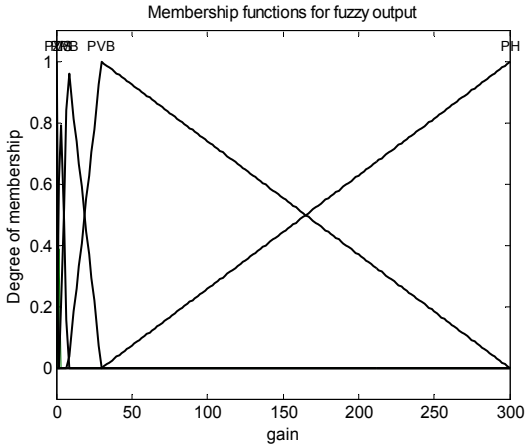

Fig. 9. Membership functions for output of the fuzzy system

TABLE III
Fuzzy tunning rules for integrator gain

Error \ Derivative of error	NB	NM	NS	Z	PS	PM	PB
NB	Z	Z	Z	PM	Z	Z	Z
NM	Z	Z	PM	PB	PM	Z	Z
NS	Z	PM	PB	PB	PB	PM	Z
Z	PM	PB	PB	PH	PB	PB	PM
PS	Z	PM	PB	PB	PB	PM	Z
PM	Z	Z	PM	PB	PM	Z	Z
PB	Z	Z	Z	PM	Z	Z	Z

VI. Simulation Results

Also in simulations, the dynamic equations of common servo motors are considered. We use on joint of the periscope to show the performance of the proposed method. Figs. 10 and 11 depict the desired and the plant response, and the tracking error for controlling the angle θ_5, respectively, when only the neural network is used as the controller. The mean-squared error is about 0.53% of the reference signal and some steady-state error can be observed.

Now, the performance of the proposed fuzzy gain scheduling will be tested. Figs. 12 and 13 show the desired, the model output, and the tracking error, respectively, when fuzzy gain scheduling is added to the control law.

The proposed fuzzy system has decrease the mean-squared tracking error from 0.53% to 0.024% while maintaining the system stability.

The fuzzy system increases the integrator gain up to 220 for the steady-state case and decreases that for the transient case(i.e. when a sudden change occurs in the tracking signal). Also, in order to show the effect of the fuzzy system, a fixed integrator gain equal to 115 has been used. As Fig. 14 shows, small change in the tracking signal has destabilized the closed-loop system.

VII. CONCLUSION

In this paper, a new Fuzzy Gain Scheduling (FGS) integrator scheme had been proposed for steady state error reduction. This scheme is parallel to main controller. Fuzzy IF-THEN rules were used to adjust the gain of the Integrator based on the system error and its derivative to reduce the steady state error along keeping total stability. This compensator system can be applied to reduce error for the other controllers that have the steady state error. Simulation results on an image stabilization platform indicated that the proposed method could reduce the steady state error of the designed main controller.

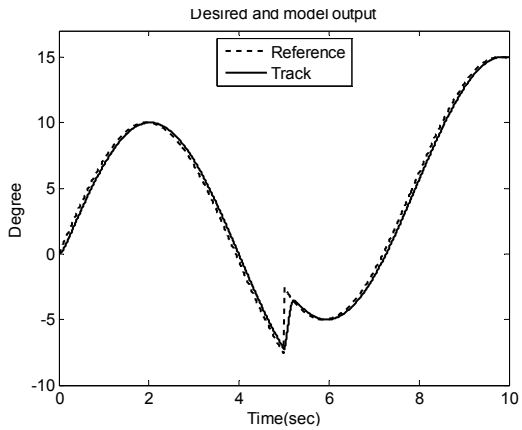

Fig. 10. Desired and model output with neural network controller

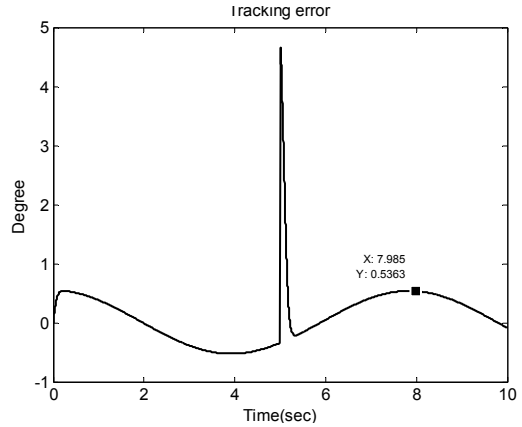

Fig. 11. Tracking error with neural network controller

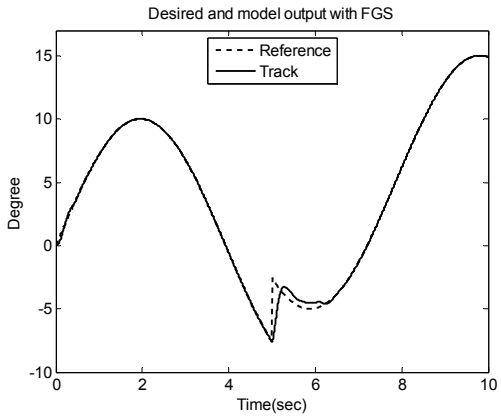

Fig. 12. Desired and model output with FGS

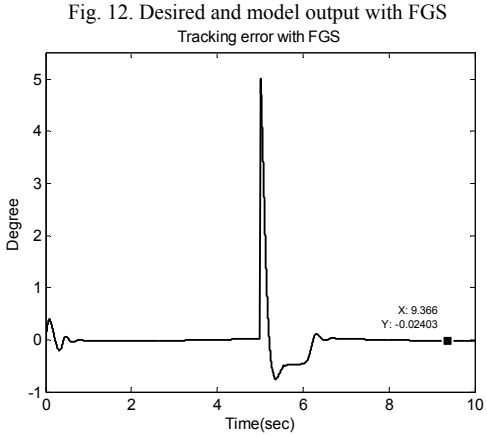

Fig. 13. Tracking error with FGS

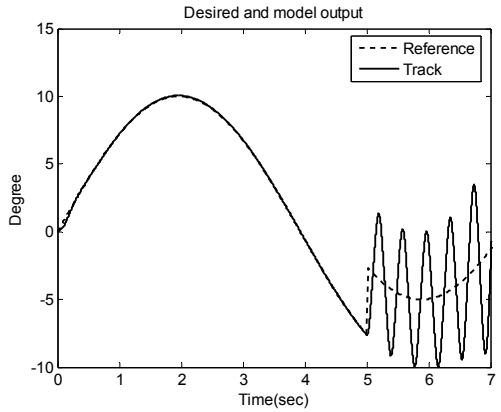

Fig. 15. .Desired and model output with neural network controller and fixed gain integrator equal to 115

REFERENCES

[1] Ping-Ho Chen, "A panoramic stabilized periscope with common optical path," pp. 183-189, 2003.

[2] T.H. Lee, K.K. Tan, A. Mamun, M.W. Lee and C.J. Khoh, "Composite control of a Gyro mirror line of sight stabilization platform design and auto-tuning," *Proceedings of IEEE 3rd World Congress on Intelligent Control and Automation*, Hefei, P.R. China, 2000.

[3] M. Harefors, *A. Study in jet engine control*, PhD thesis, Dept of Control Engineering, Chalmers University of Technology,Sweden, 1993.

[4] Passino, K. M. and S. Yurkovich (1998), *Fuzzy Control*, Menlo Park, California: Addison-Wesley.

[5] J. Craig, *Introduction to robotics: Mechanics and control*, Addison-Wesley Publishing Company, 1989.